

Automated detection of Pi2 pulsations to monitor substorm signatures: its application to real-time data and archived data

M. Nosé, T. Iyemori, M. Takeda, T. Kamei, F. Honary, S. R. Marple, J. Matzka, T. Ookawa, K. Takahashi, and G. Cifuentes-Nava

Abstract: Pi2 pulsations are defined as geomagnetic field variations with a period range of 40-150 s and an irregular waveform. It is generally accepted that Pi2 pulsations appear clearly at mid- or low-latitude ground station on the nightside in a close connection with substorm onsets. Thus nowcasting of substorm onset becomes possible, if we monitor geomagnetic field variations and detect Pi2 pulsations in real-time. We have developed an algorithm to detect Pi2 pulsations with wavelet analysis, which is suitable for investigating waves that are limited in both time and frequency, such as Pi2 pulsations. Using the geomagnetic field data from the Kakioka observatory, we have tested the algorithm and found that detection results by the algorithm on the nightside are fairly consistent with those by visual inspection. Based on this successful test result the algorithm has been applied to real-time geomagnetic field data obtained at the Mineyama and Kakioka observatories in Japan, as well as the York SAMNET station in the U. K. since 1997. We started the Pi2 detection at Fürstfeldbruck in Germany in July 2005, at APL (Applied Physics Laboratory) in the United States and Teoloyucan in Mexico in September 2005. Detection results are transferred to Kyoto University via the Internet and are available at our WWW site (<http://swdcli40.kugi.kyoto-u.ac.jp/pi2/>). The network of these 6 observatories will result in more reliable detection of Pi2 pulsations, because at least one observatory is located on the nightside at any given time. We plan to analyze archived data with this algorithm and create Pi2 database. Such database will be useful for substorm studies.

Key words: Pi2 Pulsation, Space Weather Nowcast, Real-time Geomagnetic Field Data, Substorm Database.

1. Introduction

“Pi2” designates a type of geomagnetic field oscillations which have an irregular waveform and a period in the range of 40-150 seconds. There have been a large number of studies on Pi2 pulsations since 1960s [14]. Early studies have noticed that Pi2 pulsations can be observed clearly at mid- or low-latitude ground station on the nightside when substorms were initiated [e.g., 16, 17, 18]. Since Pi2 is thought to be a good indicator of substorm onset, it has been widely used in substorm studies [e.g., 8, 9, 10]. Pi2 pulsations provide information about not only substorm occurrence but also possible longitude of substorm onset. From a longitudinal chain of ground-based magnetometers at mid-latitude, Lester et al. [4, 5, 6] found that the major axis of Pi2 polarization in the horizontal plane is ori-

ented towards the center of the substorm current wedge. This was confirmed by Gelpi et al. [2] who investigated auroral images of the DMSP satellite and the magnetic field data from the longitudinal chain at mid-latitude. Pi2 pulsations might be even related to the magnitude of substorms (i.e., substorm energy), though it is still a controversial issue. Saito and Matsushita [15] showed that the Pi2 period is correlated with the amplitude of mid-latitude positive bays. Takahashi et al. [21] demonstrated a good correlation between the Pi2 amplitude and the auroral power deduced from the ultraviolet luminosity.

Recent progress in computers and instruments for geomagnetic field measurements allows us to obtain real-time geomagnetic field data with a high time resolution less than 5 seconds (typically 1 second). If we detect Pi2 pulsations from the real-time magnetic field records, it is highly possible to obtain real-time information about substorms such as their occurrence, longitudinal location of onset, and magnitude. Thus the real-time detection of Pi2 pulsations can contribute to the space weather nowcasts.

We have developed an algorithm to detect Pi2 pulsations automatically by wavelet analysis [11] and applied it to real-time data at 6 geomagnetic observatories which are distributed in 3 different longitudinal sectors (i.e., the Far East, Europe, and North/Middle America sectors). Since the data analysis system in these observatories are on-line, detection results of Pi2 pulsations can be reported by e-mail to Kyoto University, where the results are processed immediately and become browsable from WWW. The organization of the paper is as follows. Section 2 describes brief introduction of wavelet analysis. In section 3 we show how wavelet analysis works for

Received 12 June 2006.

M. Nosé,¹ T. Iyemori, M. Takeda, and T. Kamei. Graduate School of Science, Kyoto University, Kyoto, Japan

F. Honary and S. R. Marple. Department of Communication Systems, Lancaster University, Lancaster, U. K.

J. Matzka. Department of Earth and Environmental Sciences, Ludwig-Maximilians-Universität, München, Germany

T. Ookawa. Kakioka Magnetic Observatory, Japan Meteorological Agency, Ibaraki, Japan

K. Takahashi. Applied Physics Laboratory, Johns Hopkins University, Laurel, Maryland, USA

G. Cifuentes-Nava. Instituto de Geofísica, Universidad Nacional Autónoma de México, México, D. F., Mexico

¹Corresponding author (e-mail: nose@kugi.kyoto-u.ac.jp).

geomagnetic field data. An algorithm to detect Pi2 pulsations with wavelet analysis was programmed. We show test results of the algorithm. Section 4 introduces the real-time Pi2 detection system.

2. Wavelet Analysis

Wavelet analysis is similar to Fourier analysis in that a time series is decomposed into orthonormal basis functions. Easier way to understand wavelet analysis is to describe it in comparison with Fourier analysis. Below is a brief introduction of wavelet analysis which was also described by Nosé et al. [11].

2.1. Wavelet analysis in comparison with Fourier analysis

In Fourier analysis, harmonic functions ($e^{i2\pi ft}$, where f is frequency and t is time) are adopted as orthonormal basis functions. Let $h(t)$ and $H(f)$ be a given function in the time domain and its Fourier transform in the frequency domain. The Fourier transform equations can be expressed by

$$h(t) = \int_{-\infty}^{\infty} H(f) \cdot e^{i2\pi ft} df,$$

$$H(f) = \int_{-\infty}^{\infty} h(t) \cdot (e^{i2\pi ft})^* dt,$$

where the asterisk denotes the complex conjugate. The Fourier transform is very popular in analysis of time series data, in particular, periodic signals; but it has a limitation which comes from the characteristics of the harmonic functions. Since the harmonic functions have finite values for $t \rightarrow \pm\infty$, Fourier analysis is sometimes not appropriate to analyze phenomena localized in time.

In wavelet analysis, a time series is decomposed into the orthonormal basis functions which are localized in time and limited in a specific frequency range (wavelets). Thus wavelet analysis is a suitable method for investigating the wave power of phenomena which are limited in both time and frequency, such as Pi 2 pulsations. The time series is mapped to the time-frequency domain, so the wavelet transform has two parameters which correspond to time and frequency. For a time series $x(t)$, the wavelet transform is expressed as

$$x(t) = \sum_j \sum_k \alpha_{j,k} \cdot \psi_{j,k}(t),$$

$$\alpha_{j,k} = \int_{-\infty}^{\infty} x(t) \cdot \psi_{j,k}^*(t) dt,$$

where $\alpha_{j,k}$ is the wavelet coefficient and $\psi_{j,k}(t)$ is the discrete wavelet set. $\psi_{j,k}(t)$ is constructed from an analyzing wavelet $\phi(t)$, which generates the orthonormal wavelet set, by

$$\psi_{j,k}(t) = 2^{\frac{j}{2}} \phi(2^j t - k),$$

where j and k are integers. This equation indicates that j is related to the dilation or contraction of $\phi(t)$ and k is related to the shift of $\phi(t)$ in the time domain. Thus j and k can be considered as parameters of frequency and time, respectively.

2.2. Meyer Wavelet

A number of analyzing wavelets to generate the orthonormal wavelet set have been found. For example, the Haar wavelet, the Daubechies wavelet [1], and the Meyer wavelet [7] are known. In this study we used the Meyer wavelet, because the Meyer wavelet is band-limited in frequency. The Meyer wavelet is expressed as follows [19, 20, 22, 23, 24]:

$$\phi(t) = \frac{1}{2\pi} \int_{-\infty}^{\infty} \Phi(\omega) e^{i\omega t} d\omega,$$

where ω is angular frequency and

$$\Phi(\omega) = \begin{cases} 0 & (|\omega| \geq \frac{8}{3}\pi) \\ e^{-i\frac{\omega}{2}} \left[1 + \exp \left\{ \frac{32}{3}\pi \frac{|\omega| - 2\pi}{(|\omega| - \frac{8}{3}\pi)^2 (|\omega| - \frac{4}{3}\pi)^2} \right\} \right]^{-\frac{1}{2}} & (\frac{4}{3}\pi < |\omega| < \frac{8}{3}\pi) \\ e^{-i\frac{\omega}{2}} & (|\omega| = \frac{4}{3}\pi) \\ e^{-i\frac{\omega}{2}} \left[1 + \exp \left\{ -\frac{4}{3}\pi \frac{|\omega| - \pi}{(|\omega| - \frac{4}{3}\pi)^2 (|\omega| - \frac{2}{3}\pi)^2} \right\} \right]^{-\frac{1}{2}} & (\frac{2}{3}\pi < |\omega| < \frac{4}{3}\pi) \\ 0 & (0 \leq |\omega| \leq \frac{2}{3}\pi) \end{cases}.$$

For actual analysis we use a discrete time series and take a finite data segment. Assuming a time series which has a sampling rate dt and a number of data points N ($N=2^n$, n is integer), we will obtain wavelet coefficients $\alpha_{j,k}$ confined in $0 \leq j \leq n-1$ and $0 \leq k \leq 2^j - 1$. The frequency band for each j is $2^j/3T \leq f \leq 2^{j+2}/3T$, where T is the data length ($T=Ndt$). Note that the widths of time window and frequency window covered by $\alpha_{j,k}$ are $T/2^j$ and $2^j/T$, respectively. This indicates that the wavelet coefficient with a large value of j has high resolution in time and low resolution in frequency, and vice versa. The Nyquist frequency is included in the frequency range supported by the maximum value of j . Figure 1 shows

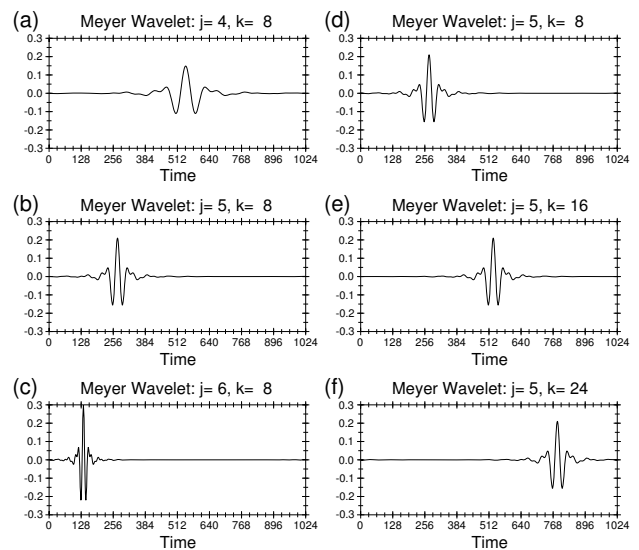


Fig. 1. Wavelet functions $\psi_{j,k}(t)$ which are generated from the Meyer wavelet with $N=1024$ and (j, k) of (a) (4,8), (b) (5,8), (c) (6,8), (d) (5,8), (e) (5,16), and (f) (5,24).

waveforms of the wavelet functions $\psi_{j,k}(t)$ which are generated from the Meyer wavelet with $N=1024=2^{10}$. Note that the Meyer wavelet has a symmetric waveform. From Figures 1a-1c which give examples of wavelet functions with different values of j (i.e., $j=4-6$), we see that the wavelet function with a smaller value of j is more dilated than that with a larger value of j . Figures 1d-1f display examples of wavelet functions with different values of k (i.e., $k=8, 16, 24$). For a smaller value of k , the non-zero part of the wavelet function appears earlier in time. Therefore we can discuss phenomena from the viewpoint of both frequency (j) and time (k) at once. Even if more than one wave packets having an identical frequency appear at different times, these phenomena are identified by wavelet coefficients with different values of k .

3. Wavelet Analysis of Geomagnetic Field Data

3.1. Pi2 pulsation at 1620 UT on 29 March 2006

We applied the wavelet analysis to geomagnetic field data obtained at Kakioka (27.37° geomagnetic latitude (GMLAT), 208.71° geomagnetic longitude (GMLON)) with a sampling rate of 1 second. Figure 2 shows an example of the wavelet analysis for data around 1620 UT on March 29, 2006, when the Eighth International Conference on Substorms was held at Banff, Canada. The left panels of Figures 2a-2e display the geomagnetic field variations in the H-component for 512 seconds before the time indicated in the top of each panel. Note that time proceeds forward in 1-minute steps from Figure 2a to Figure 2c, while in 2-minute time steps from Figure 2c to Figure 2e. We found that a Pi2 pulsation with the period of ~ 100 seconds ($f \sim 10$ mHz) appeared at 1620-1621 UT.

The right panels show the absolute values of normalized wavelet coefficients $\sqrt{2^j/T}|\alpha_{j,k}|$ with $j=4-6$ corresponding to the geomagnetic field data in the left panels. The frequency ranges of wavelet functions with $j=4-6$ are 5.2-20.8 mHz, 10.4-41.7 mHz, and 20.8-83.3 mHz, respectively. Pi2 pulsations which have a frequency range of 6.67-25.0 mHz are mainly represented by wavelet coefficients with $j=4$ and 5. (Careful readers may notice that the aforementioned frequency ranges are derived in the case of $N=1024$. This is because we added 256 data points artificially to both ends of the 512-second data segment before wavelet analysis; the additional data are given to be equal to each end of the data segment. This data processing is necessary to obtain appropriate wavelet coefficients, in particular, when the geomagnetic field data at both ends are largely different.) In the right panels of Figures 2b-2e we find some wavelet coefficients having values larger than 0.5, which are indicated by shading. These wavelet coefficients appeared only in the time intervals when the Pi2 pulsation was initiated and only at $j=4$ which covers the frequency of the Pi2 pulsation (~ 10 mHz). Therefore we can identify Pi2 pulsations by detecting large wavelet coefficients for $j=4$ and 5 (or possibly $j=6$). The detection criteria (i.e., magnitude of wavelet coefficients, etc.) will be determined empirically and depend on geomagnetic observatories.

3.2. Pi2 detection algorithm

We have developed an algorithm to detect Pi2 pulsations automatically. The algorithm basically consists of procedures

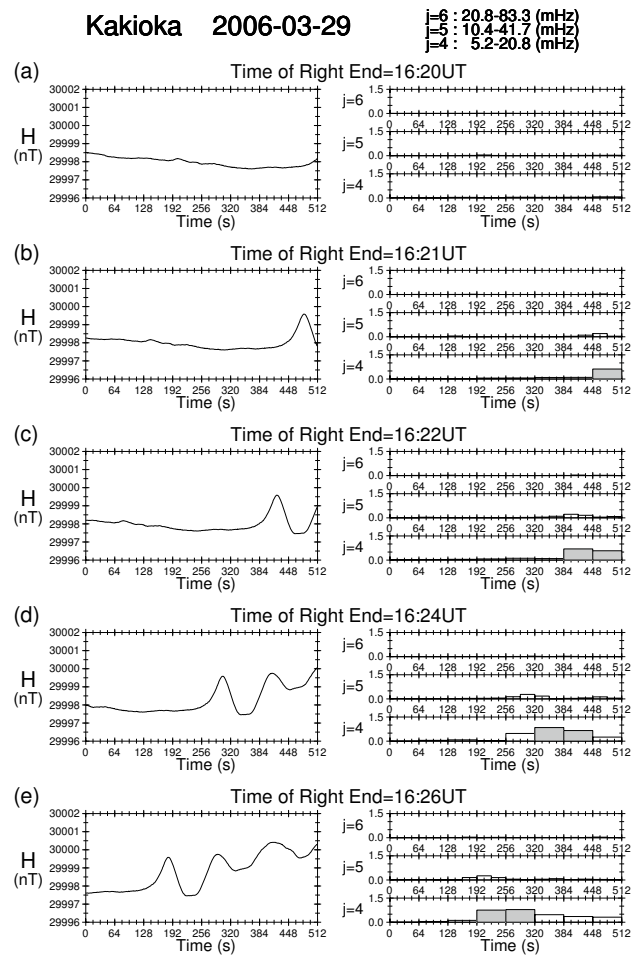


Fig. 2. Examples of wavelet analysis for the geomagnetic field data. (a) The left panel indicates the geomagnetic field variations in the H-component at Kakioka for 512 seconds before 1620 UT. The right panel shows the absolute values of normalized wavelet coefficients $\sqrt{2^j/T}|\alpha_{j,k}|$ with $j=4-6$ corresponding to the geomagnetic field data in the left panel. (b)-(e) Same as Figure 2a except for time of the right end of 1621 UT, 1622 UT, 1624 UT, and 1626 UT, respectively. Wavelet coefficients with values of ≥ 0.5 are indicated by shading.

to analyze the H- and D-components of the geomagnetic field data with the Meyer wavelet and to detect wavelet coefficients with $j=4$ and 5 which exceed the detection criterion. From the wavelet coefficients we can estimate the amplitude of events. Thus the detection criterion was chosen as events having a peak-to-peak amplitude larger than 0.6 nT are identified. We tested the algorithm using the geomagnetic field data from Kakioka on the nightside (from 1800 magnetic local time (MLT) through midnight to 0400 MLT) in the period of January 2001. The data segment was taken to be 512-second long and was shifted forward by 60 seconds at every analysis, such as Figures 2a-2c. Events detected by the algorithm were visually inspected if they are real Pi2 pulsations.

A test result of the algorithm is summarized in Table 1. The detection algorithm found 90 possible Pi2 pulsations. We classified these events into 4 categories according to the estimated

Kakioka January 2001 1800-0400 MLT		Program Detection [Wavelet Analysis]				
		0.6-1.2 nT	1.2-1.8 nT	1.8-3.0 nT	3.0 nT-	Total
		64	13	9	4	90
Visual Inspection	Pi2	52	13	9	4	78
	Non Pi2	12	0	0	0	12
Rate of Successful Detection		81.3%	100%	100%	100%	86.7%

Table 1. Test result of the Pi2 detection algorithm for the Kakioka data in the nighttime (1800-0400 MLT) in January 2001.

peak-to-peak amplitudes, that is, 0.6-1.2 nT, 1.2-1.8 nT, 1.8 nT-3.0 nT, and larger than 3.0 nT. From the table we found that all of events with amplitude larger than 1.2 nT (i.e., 26 events) were Pi2 pulsations. However, 12 out of 64 events with amplitude of 0.6-1.2 nT were not real Pi2 pulsations. Thus the rate of successful detection is calculated to be 86.7% ((90-12)/90). We consider that the Pi2 detection algorithm gives fairly good results on the nightside (1800-0400 MLT). It is worth mentioning here that geomagnetic condition during January 2001 was quiet (monthly averages of Kp and Dst indices were 2- and -8.7 nT, respectively). During more disturbed period the rate of successful detection might become lower, because the geomagnetic field variations in such period often involve a lot of disturbances in the Pi2 frequency band.

4. Automated Detection of Pi2 Pulsations

4.1. Real-time Pi2 detection system

We have applied the Pi2 detection algorithm to real-time geomagnetic field data obtained at low- and mid-latitude observatories. The algorithm has been implemented in the on-site computers at the Mineyama observatory in Japan since February 1996 and at the York SAMNET station in the U. K. since May 1997 [11]. Real-time Pi2 detection was started also at the Fürstenfeldbruck observatory in Germany in July 2005 as well as at APL (Applied Physics Laboratory) in the United States and the Teoloyucan observatory in Mexico in September 2005. The coordinates and locations of these 6 observatories were

Station	(degree)			
	GGLAT	GGLON	GMLAT ¹	GMLON ¹
Mineyama	35.57	135.05	26.31	204.14
Kakioka	36.23	140.19	27.37	208.71
York	53.95	358.95	56.12	85.09
Fürstenfeldbruck	48.17	11.28	48.39	94.56
APL	39.17	283.12	49.37	353.87
Teoloyucan	19.75	260.82	28.76	330.34

¹ Values in January 2005

Table 2. Coordinates of observatories where the Pi2 detection algorithm is applied to real-time geomagnetic field data. GGLAT and GGLON denotes geographic latitude and longitude. GMLAT and GMLON means geomagnetic latitude and longitude.

shown in Table 2 and Figure 3. All observatories are located in low- and mid-latitude of the northern hemisphere (26°-56° GMLAT). It is noted that the observatories form a pair in 3 different longitudinal sectors (i.e., the Far East, Europe, and North/Middle America sectors) which were separated by about 120° in geomagnetic longitude. Thus at a given time at least one pair of observatories is located on the nightside where Pi2 pulsations are predominantly observed. A pair of observatories provides a more robust detection of Pi2 pulsations, because occurrence probability of entire data loss in a given sector becomes lower in the case of two observatories than a single observatory.

When Pi2 pulsations were detected by the algorithm, results of detection (i.e., onset time, estimated amplitude, and waveform) are immediately transferred by e-mail to Kyoto University, Japan. The results of real-time Pi2 detection are available from the WWW site (<http://swdcli40.kugi.kyoto-u.ac.jp/pi2/>).

Location of observatories in geomagnetic coordinates

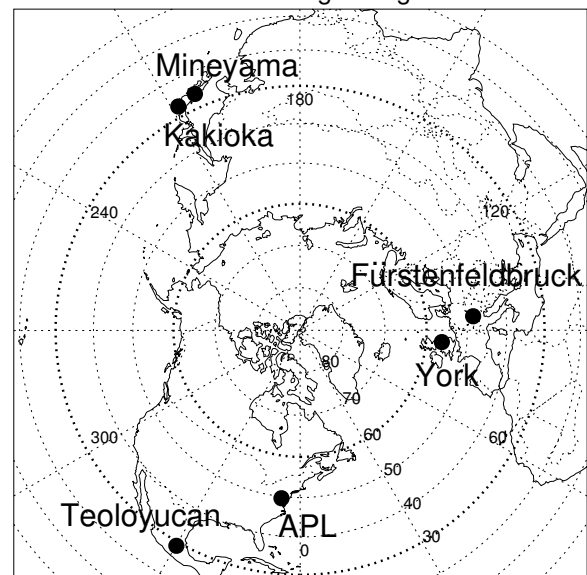


Fig. 3. Location of observatories in geomagnetic coordinates where the Pi2 detection algorithm is applied to real-time geomagnetic field data. Latitudinal circles of GMLAT=30° and 60° are shown with thick-dotted lines.

4.2. Examples of Pi2 detection

Figures 4a-4c show examples of Pi2 pulsations which were identified by the real-time Pi2 detection system. In each panel we plotted the H-component of the geomagnetic field data from two observatories which were at different magnetic local time (MLT); that is, the nightside (21-23 MLT) for the top and the dayside (12-13 MLT) or the dawn side (~06 MLT) for the bottom. A triangle indicates the onset time which was reported by the detection algorithm in each observatory. A Pi2 pulsation occurrence was reported from Fürstenfeldbruck and Teoloyucan at 1907 UT on May 21, 2006, which is consistent with the visual detection (Figure 4a). Note that time resolution at

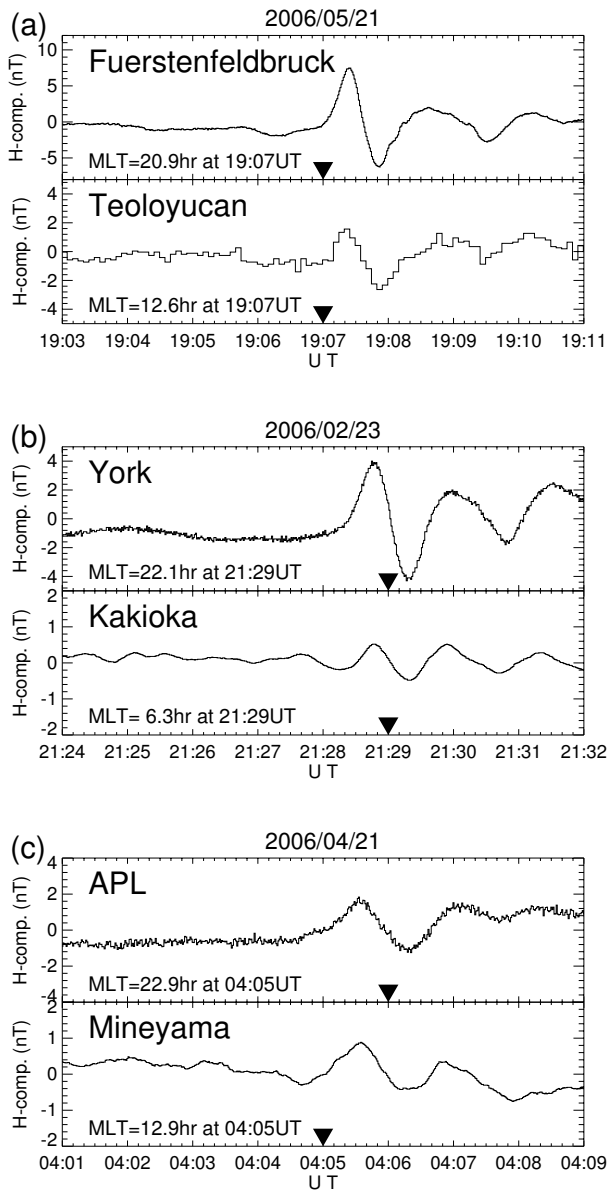


Fig. 4. Examples of Pi2 pulsations identified by the real-time Pi2 detection system in two different longitude; (a) Fürstenfeldbruck and Teoloyucan, (b) York and Kakioka, and (c) APL and Mineyama.

Fürstenfeldbruck is 1 second, while that at Teoloyucan is 5 seconds. Figure 4b shows that the detection system identified a Pi2 pulsation at 2129 UT on February 23, 2006 at both York and Kakioka. In Figure 4c there was a 1 minute difference in the reported onset time between APL and Mineyama, though we visually identify onset time of the Pi2 pulsation at 0405 UT on April 21, 2006.

These events reveal that Pi2 pulsations can be observed in two different longitudinal sectors, even if observatories are separated by 8-10 hours of MLT. It is also found that the Pi2 pulsations in Figure 4 have no clear phase difference between the observatories, implying that the longitudinal wave number of the pulsation is ~0. These results are consistent with those by Kitamura et al. [3] and Nosé et al. [12, 13].

4.3. Pi2 database

As can be seen in Table 1 or Figure 4, the algorithm developed in this study provides a rather good result of Pi2 detection. Thus we plan to analyze archived geomagnetic field data with this algorithm and create database of Pi2 pulsations. The database will be useful for substorm studies and will become available from our WWW server in future.

Acknowledgements

We thank Sven Egdorf, Martin Feller, Bruce Toth, Simon Wing, Linda Burke, and Mark Moldwin for their help in maintaining the Pi2 detection system. This work was supported by the Ministry of Education, Science, Sports and Culture, Grant-in-Aid for Young Scientists (B) (grant 17740327) and the Kurata Memorial Hitachi Science and Technology Foundation (grant 844). Work at JHU/APL was supported by NASA under grant NAG5-13119.

References

1. Daubechies, I., Orthonormal bases of compactly supported wavelets, *Comm. Pure Appl. Math.*, 41, 909-996, 1988.
2. Gelpi, C., H. J. Singer, and W. J. Hughes, A comparison of magnetic signatures and DMSP auroral images at substorm onset: Three case studies, *J. Geophys. Res.*, 92, 2447-2460, 1987.
3. Kitamura, T., O. Saka, M. Shimoizumi, H. Tachihara, T. Oguti, T. Araki, N. Sato, M. Ishitsuka, O. Veliz, and J. B. Nyobe, Global mode of Pi2 waves in the equatorial region: Difference of Pi2 mode between high and equatorial latitudes, *J. Geomagn. Geoelectr.*, 40, 621-634, 1988.
4. Lester, M., W. J. Hughes, and H. J. Singer, Polarization patterns of Pi2 magnetic pulsations and the substorm current wedge, *J. Geophys. Res.*, 88, 7958-7966, 1983.
5. Lester, M., W. J. Hughes, and H. J. Singer, Longitudinal structure in Pi2 pulsations and the substorm current wedge, *J. Geophys. Res.*, 89, 5489-5494, 1984.
6. Lester, M., H. J. Singer, D. P. Smith, and W. J. Hughes, Pi2 pulsations and the substorm current wedge: Low-latitude polarization, *J. Geophys. Res.*, 94, 17,133-17,141, 1989.
7. Meyer, Y., Orthonormal wavelets, in *Wavelets*, edited by J. M. Combes, A. Grossmann, and Ph. Tchamitchian, pp. 21-37, Springer-Verlag, Berlin, 1989.

8. Miyashita, Y., S. Machida, A. Nishida, T. Mukai, Y. Saito, and S. Kokubun, Geotail observations of total pressure and electric field variations in the near and mid-distant tail associated with substorm onsets, *J. Geophys. Res.*, *26*, 639-642, 1999.
9. Miyashita, Y., S. Machida, T. Mukai, Y. Saito, K. Tsuruda, H. Hayakawa, and P. R. Sutcliffe, A statistical study of variations in the near and middistant magnetotail associated with substorm onsets: GEOTAIL observations, *J. Geophys. Res.*, *105*, 15,913-15,930, 2000.
10. Nagai, T., M. Fujimoto, Y. Saito, S. Machida, T. Terasawa, R. Nakamura, T. Yamamoto, T. Mukai, A. Nishida, and S. Kokubun, *J. Geophys. Res.*, *103*, 4419-4440, 1998.
11. Nosé, M., T. Iyemori, M. Takeda, T. Kamei, D. K. Milling, D. Orr, H. J. Singer, E. W. Worthington, and N. Sumitomo, Automated detection of Pi 2 pulsations using wavelet analysis: 1. Method and an application for substorm monitoring, *Earth Planet. Space*, *50*, 773-783, 1998.
12. Nosé, M., K. Takahashi, T. Uozumi, K. Yumoto, Y. Miyoshi, A. Morioka, D. K. Milling, P. R. Sutcliffe, H. Matsumoto, T. Goka, and H. Nakata, Multipoint observations of a Pi2 pulsation on morning side: The 20 September 1995 event, *J. Geophys. Res.*, *108*, 1219, doi:10.1029/2002JA009747, 2003.
13. Nosé, M., K. Liou, P. R. Sutcliffe, Longitudinal dependence of characteristics of low-latitude Pi2 pulsations observed at Kakioka and Hermanus, *Earth Planet. Space*, *58*, 775-783, 2006.
14. Saito, T., Geomagnetic pulsations, *Space Sci. Rev.*, *10*, 319-412, 1969.
15. Saito, T. and S. Matsushita, Solar cycle effects on geomagnetic Pi2 pulsations, *J. Geophys. Res.*, *73*, 267-286, 1968.
16. Saito, T., T. Sakurai, and Y. Koyama, Mechanism of association between Pi 2 pulsation and magnetospheric substorm, *J. Atmos. Terr. Phys.*, *38*, 1265-1277, 1976a.
17. Saito, T., K. Yumoto, and Y. Koyama, Magnetic pulsation Pi 2 as a sensitive indicator of magnetospheric substorm, *Planet. Space Sci.*, *24*, 1025-1029, 1976b.
18. Sakurai, T. and T. Saito, Magnetic pulsation Pi 2 and substorm onset, *Planet. Space Sci.*, *24*, 573-575, 1976.
19. Sasaki, F., T. Maeda, and M. Yamada, Study of time history data using wavelet transform, *J. Struc. Eng. Architec. Inst. Japan*, *38B*, 9-20, 1992 (in Japanese with English abstract).
20. Sato, K. and M. Yamada, Vertical structure of atmospheric gravity waves revealed by the wavelet analysis, *J. Geophys. Res.*, *99*, 20,623-20,631, 1994.
21. Takahashi, K., K. Liou, and K. Yumoto, Correlative study of ultraviolet aurora and low-latitude Pi2 pulsations, *J. Geophys. Res.*, *107*, 1417, doi:10.1029/2002JA009455, 2002.
22. Yamada, M. and K. Ohkitani, Orthonormal wavelet analysis of turbulence, *Fluid Dyn. Res.*, *8*, 101-115, 1991.
23. Yamanaka, M. D., T. Shimomai, and S. Fukao, A model of quasi-monochromatic field of middle-atmospheric internal gravity waves, *Proc. of the 1992 STEP Symposium/5th COSPAR Colloquium*, 511-518, 1994.
24. Yomogida, K., Detection of anomalous seismic phases by the wavelet transform, *Geophys. J. Int.*, *116*, 119-130, 1994.